

## Magnetic trapping of ytterbium and the alkaline-earth metals

T. Loftus,\* J. R. Bochinski,\* and T. W. Mossberg

Oregon Center for Optics and Department of Physics, University of Oregon, Eugene, Oregon 97403

(Received 8 June 2001; published 29 July 2002)

Atomic ytterbium (Yb), magnesium (Mg), calcium (Ca), and strontium (Sr) possess a simple yet versatile internal level structure and a diversity of naturally abundant fermionic and bosonic isotopes, making these systems ideal for studies of cold collisions and weakly interacting quantum degenerate gases. Unlike alkali-metal atoms, however, Yb, Mg, Ca, and Sr cannot be magnetically trapped in the ground state. We analyze a solution to this problem involving magnetic trapping in a low-lying metastable excited state and predict that significant magnetic trap populations can be obtained via continuous, *in situ* loading from Yb and Sr  $^1S_0 - ^1P_1$  magneto-optical traps.

DOI: 10.1103/PhysRevA.66.013411

PACS number(s): 32.80.Pj

Magnetic trapping of ground-state neutral atoms [1] has enabled unique explorations into two-body interatomic interactions [2] and collisions [3], radio-frequency and optical spectroscopy [4], trapped atom laser-induced [5] and evaporative cooling [6], and weakly interacting quantum degenerate gases [7,8]. Atomic ytterbium (Yb) and the alkaline-earth atoms magnesium (Mg), calcium (Ca), and strontium (Sr) [hereafter collectively labeled singlet-triplet (ST) atoms] possess a diversity of naturally abundant fermionic and bosonic isotopes [9], spectrally narrow transitions that enable ultralow temperature, high spatial density laser cooling [10–12], and a simple internal level structure ideally suited to quantitative studies of cold collisions [13]. As such, ST atoms offer unique opportunities for future studies of magnetically trapped samples. Lacking the requisite ground-state magnetic substructure, however, ST atoms cannot be held in ground-state magnetic traps.

In this paper we analyze the solution to this problem proposed by Loftus *et al.* [14] which relies on magnetically trapping ST atoms in the low-lying  $^3P_2$  ( $m_J=2$ ) weak-field seeking metastable [15–18] excited-state. We begin by showing that for each ST atom a single magnetic field supports *both* a  $^1S_0 - ^1P_1$  transition magneto-optical trap (MOT) and a pure magnetic trap capable of holding  $^1S_0 - ^1P_1$  MOT-cooled atoms. Next, we discuss three *in situ* techniques for loading  $^3P_2$  ( $m_J=2$ ) magnetic traps with atoms precooled in  $^1S_0 - ^1P_1$  or  $^1S_0 - ^3P_1$  MOTs and provide numerical estimates, based on the relevant Zeeman substate dependent decay paths [19], for the resulting magnetic trap loading rates. Finally, we discuss a zero-background technique for observing the magnetically trapped atoms. For simplicity, our discussion is confined to magnetic trapping of the most abundant, even atomic mass number ST atom isotopes. Note, however, that the procedures outlined here are applicable to the remaining isotopes, even those with nonzero nuclear spin.

Figure 1(a) shows a contour plot (calculated according to analytic expressions given by Bergman *et al.* [20]) of the typical anti-Helmholtz magnetic field used for a previously

reported  $^1S_0 - ^1P_1$  Yb MOT (60 G/cm axial field gradient) [14,21]. In the figure, coil windings lie in the centers of the four black dots and equimagnitude field contours are labeled in Gauss. The spatial extent of a magnetic trap employing this field is set by the direction-dependent radius of the maximum closed contour centered about the magnetic field null. We label the magnitude of this contour  $B_M$  where in Fig. 1(a),  $B_M=40$  G. In Fig. 1(b) we plot the  $^3P_2$  ( $m_J=2$ ) magnetic trap depth for each species as a function of  $B_M$ . The trap depth is scaled by  $T_S$ , the species specific  $^1S_0 - ^1P_1$  Doppler-limited MOT temperature. The inset shows the trap depth normalized by  $T_T$ , the species specific  $^1S_0 - ^3P_1$

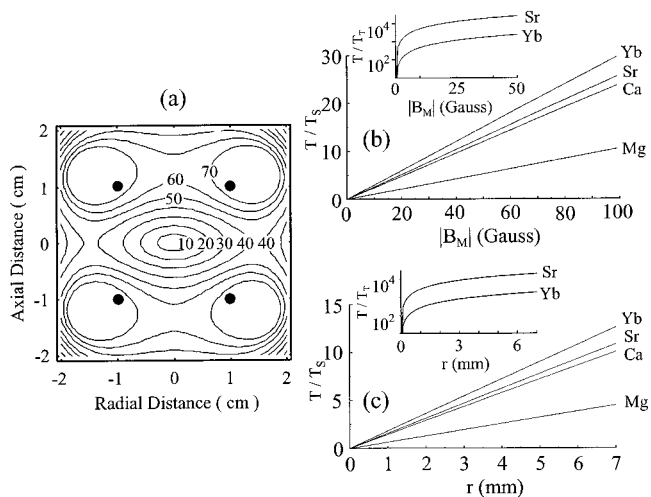


FIG. 1. (a) Contour plot of the anti-Helmholtz magnetic field used for a previously reported  $^1S_0 - ^1P_1$  Yb MOT [14]. Coil windings lie in the centers of the four black dots and equimagnitude field contours are labeled in Gauss. (b)  $^3P_2$  ( $m_J=2$ ) magnetic trap depth as a function of  $B_M$ , the maximum effective trap field [ $\sim 40$  G in Fig. 1(a)]. The trap depth is scaled by  $T_S$ , the species specific  $^1S_0 - ^1P_1$  Doppler-limited MOT temperature. (c)  $^3P_2$  ( $m_J=2$ ) magnetic trap depth versus the trap size,  $r$ , with a fixed axial field gradient of 60 G/cm [the axial gradient in (a)]. Here,  $r$  is measured relative to the magnetic field null point. Insets to (b) and (c) show the  $^3P_2$  ( $m_J=2$ ) magnetic trap depth normalized by  $T_T$ , the species specific  $^1S_0 - ^3P_1$  Doppler limited [22] temperatures for Yb and Sr. Note that a field gradient of  $\sim 10$  G/cm ( $\sim 5$  G/cm) is required to suspend Yb (Sr) atoms against gravity.

\*Present address: JILA, National Institute of Standards and Technology and University of Colorado, Boulder, CO 80309.

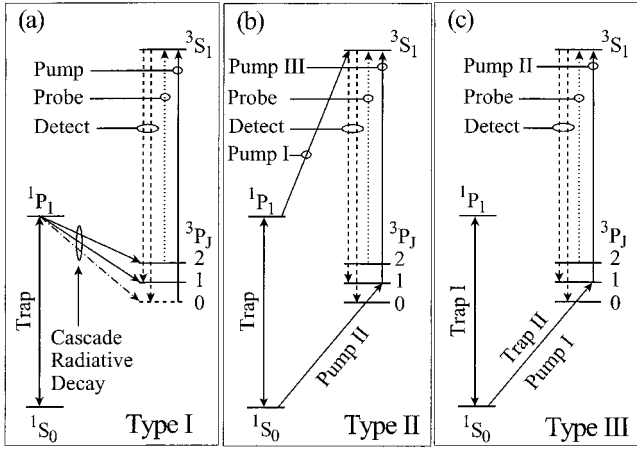


FIG. 2. Simplified energy-level diagrams showing (a) type I, (b) type II, and (c), type III transfer processes and a zero-background technique for observing atoms magnetically trapped in the  $^3P_2$  ( $m_J=2$ ) state. In (a), transitions and states labeled with dotted-dashed lines apply only to Yb. In (b), Pump I (Pump II and Pump III) is used for incoherent (semicoherent) transfer. For all three, the detection (probe) transitions are denoted by dashed (dotted) lines.

Doppler-limited [22] temperatures for Yb and Sr. Figure 1(c) depicts the  $^3P_2$  ( $m_J=2$ ) magnetic trap depth as a function of the trap size,  $r$ , for a fixed axial magnetic field gradient of 60 G/cm. Here,  $r$  is measured relative to the magnetic field null point [note that in Fig. 1(a),  $r_{\max} \sim 7$  mm along the axial direction]. For all four species the magnetic trap shown in Fig. 1(a) is deep enough to capture precooled ST atoms, even those that are only cooled to  $T_S$ .

Figure 2 presents three techniques for loading ST atoms into a  $^3P_2$  ( $m_J=2$ ) magnetic trap. Type I transfer [Fig. 2(a)] uses a  $^1S_0-^1P_1$  MOT to simultaneously precool the ST atoms and, through radiative branching induced MOT loss [23], load the atoms into the  $^3P_2$  ( $m_J=2$ ) state. In contrast, type II (type III) transfer employs  $^1S_0-^1P_1$  ( $^1S_0-^3P_1$ ) MOT precooling followed by population transfer to the  $^3P_2$  ( $m_J=2$ ) state via optical pumping. As discussed below, all three transfer schemes are applicable to Yb, Ca, and Sr while, due to the details of the Mg internal level structure, Mg requires the use of type II or type III transfer. Note that in all cases approximately equal populations are loaded into the  $^3P_2$  ( $m_J=2$ ) and  $^3P_2$  ( $m_J=1$ ) weak-field seeking states. As demonstrated elsewhere [8], however, the resulting spin-mixed sample could be purified by ejecting  $^3P_2$  ( $m_J=1$ ) atoms from the magnetic trap with a swept-frequency rf field. The remainder of our discussion, therefore, will focus on atoms loaded into the more tightly confined  $^3P_2$  ( $m_J=2$ ) state. In the following, we write the continuous or quasi-continuous type I and type II transfer rates,  $R_M$ , as  $R_M = f(N_S/\tau_S) = R_S f$  where  $f < 1$  is an effective  $^1P_1 \rightarrow ^3P_2$  ( $m_J=2$ ) or  $^3S_1 \rightarrow ^3P_2$  ( $m_J=2$ ) cascade decay fraction,  $N_S$  ( $\tau_S$ ) is the population (lifetime) of a  $^1S_0-^1P_1$  MOT, and  $R_S$  is a  $^1S_0-^1P_1$  MOT loading rate. Type III loading, which involves transferring population from a  $^1S_0-^3P_1$  MOT to the  $^3P_2$  ( $m_J=2$ ) state in a pulsed manner, is characterized by  $f'N_T$  where  $f' < 1$  is a  $^3P_2$  ( $m_J=2$ ) transfer fraction and  $N_T$  is the steady-state population of a  $^1S_0-^3P_1$  MOT. Note

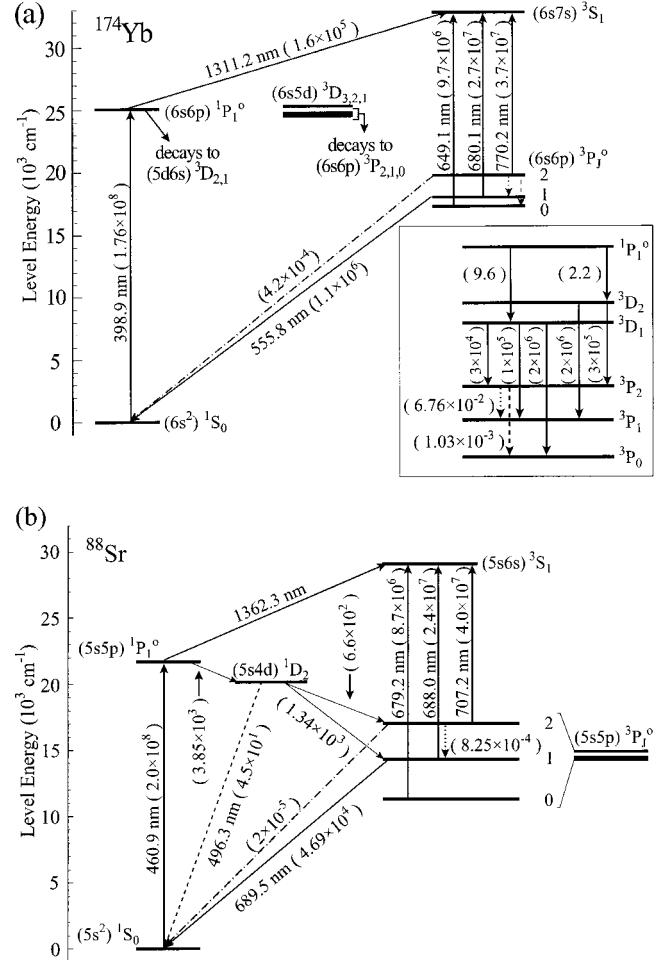


FIG. 3. Simplified energy-level diagrams for (a) Yb and (b) Sr. Electric dipole and quadrupole and magnetic dipole and quadrupole transitions are represented by solid, dashed, dotted, and dotted-dashed lines, respectively. States with a superscript  $o$  have odd parity, transition wavelengths are given in vacuum [24,25], and numbers in parentheses give transition probabilities (in  $s^{-1}$ ) [16–18, 27–31]. The inset in (a) shows an expanded view of the Yb  $^1P_1 \rightarrow ^3D_{2,1} \rightarrow ^3P_{2,1,0}$  decay channel.

that  $f$  and  $f'$  depend on spontaneous decay rates and Zeeman substate dependent weighting factors. For the former, we use either measured or theoretically predicted values (see Fig. 3 and Refs. [13,16,17,24–32]) while the latter are calculated according to the Wigner-Eckhart theorem [33].

In type I and type II transfer [Figs. 2(a) and 2(b), respectively], the atoms are initially loaded into  $^1S_0-^1P_1$  MOTs. Type I transfer then consists of allowing the atoms to radiatively cascade from the  $^1P_1$  state to the  $^3P_2$  ( $m_J=2$ ) state while they are held in the  $^1S_0-^1P_1$  MOT. Note that in this case  $\tau_c < \tau_S/1000$  for all four ST atoms where  $\tau_c$  is the time required to slow atoms from the MOT capture velocity to  $T_S$ . Thus the atoms are generally cooled to  $T_S$  before the radiative cascade from the  $^1P_1$  state to the  $^3P_2$  ( $m_J=2$ ) state occurs. For Yb and Sr, this transfer scheme is relatively efficient (see Table I) since cascade radiative decay from the  $^1P_1$  state which terminates in the  $^3P_{2,0}$  states ( $^3P_2$  state) is

TABLE I. Estimated  $^3P_2$  ( $m_J=2$ ) state transfer fraction  $f$  for the continuous and quasicontinuous type I and type II transfer processes. The  $f$  value given for type II loading assumes a semicoherent, stepwise transfer to the  $^3P_2$  ( $m_J=2$ ) state; the incoherent type II transfer fraction  $f$  is smaller by roughly a factor of 3.

Loading scheme	Species	$f$
Type I	$^{174}\text{Yb}$	without repumping: 0.01 with repumping: 0.1
	$^{40}\text{Ca}$	0.2
	$^{88}\text{Sr}$	0.2
Type II	$^{174}\text{Yb}$	0.3
	$^{24}\text{Mg}$	
	$^{40}\text{Ca}$	
	$^{88}\text{Sr}$	

the dominant Yb (Sr)  $^1S_0-^1P_1$  MOT loss mechanism [10,11,23] and intermediate states decay quickly to the  $^3P_2$  state [see Figs. 3(a) and 3(b)]. Using the  $N_s$  and  $\tau_s$  values reported for Sr in Ref. [11], for example, gives  $R_M \sim 10^9$  atoms/s. Moreover, in Yb the transfer efficiency can be increased approximately an order of magnitude by optically pumping population from the  $^3P_0$  state to the  $^3P_2$  ( $m_J=2$ ) through excitation of the  $^3P_0-^3S_1$  transition [see Fig. 3(a)]. As shown in Table I, type I transfer is similarly efficient for Ca. Note, however, that cold Ca atoms lost from a  $^1S_0-^1P_1$  MOT via radiative decay spend  $\sim 10$  ms in the intermediate  $^1D_2$  state [Ca Einstein  $A(^1D_2-^3P_2) = 92.9 \text{ s}^{-1}$  [28]], a process that increases the  $^3P_2$  ( $m_J=2$ ) cloud size [using the conservative force experienced by  $^1D_2$  state atoms in the Fig. 1(a) field, the atoms travel  $\sim 1$  mm prior to  $^1D_2-^3P_2$  decay] and results in additional heating [approximately a factor of 2 along the Fig. 1(a) trap axial direction]. Finally, note that type I transfer cannot be used for Mg since in this case the  $^1S_0-^1P_1$  transition is radiatively closed [34].

In type II transfer, these limitations are overcome by optically pumping  $^1S_0-^1P_1$  MOT precooled atoms to the  $^3P_2$  ( $m_J=2$ ) state via radiative decay from the  $^3S_1$  state, a process that can be accomplished two ways. First, exciting the  $^1P_1-^3S_1$  transition with a Rabi frequency,  $\Omega \gg 1/\tau_p$  where  $\tau_p$  is the  $^3S_1$  state lifetime, equalizes the  $^1P_1$  and  $^3S_1$  state populations and fills the  $^3P_2$  ( $m_J=2$ ) state with a  $1/e$  time of  $\sim \tau_p$ . This incoherent population transfer is continued until the  $^1S_0-^1P_1$  MOT is emptied, can be repeated once every  $\tau_s$  (note  $\tau_s, \tau_c \gg \tau_p$ ), and assuming equal population distributions in the  $^1P_1$  and  $^3S_1$  magnetic substates, gives  $f \sim 0.1$  for all four ST atom species. Alternatively, once every  $\tau_s$ , the  $^1S_0-^1P_1$  MOT optical fields are extinguished and temporally separated, circularly polarized  $\pi$  pulses excite the stepwise  $^1S_0 \rightarrow ^3P_1$  ( $m_J=1$ )  $\rightarrow ^3S_1$  ( $m_J=1$ ) transition. Subsequently, radiative decay from the  $^3S_1$  ( $m_J=1$ ) state loads the atoms into the  $^3P_2$  ( $m_J=2$ ) state. This semicoherent process enhances the type II transfer efficiency by roughly a factor of 3 and due to the spectral width of the  $^1S_0-^3P_1$  transition, enables additional one-dimensional cooling

[10,35]. Moreover, the resulting magnetic trap spin mixture favors atoms in the  $^3P_2$  ( $m_J=2$ ) state over atoms in the  $^3P_2$  ( $m_J=1$ ) state by a factor of 2.

Lastly, in type III transfer, the atoms are precooled in  $^1S_0-^3P_1$  MOTs loaded with either a  $^1S_0-^1P_1$  MOT [10,11] or a Zeeman slowed atomic beam [12]. The MOT optical and magnetic fields are then turned off, polarized  $\pi$  pulses load atoms into the  $^3P_2$  ( $m_J=2$ ) state by exciting the stepwise  $^1S_0 \rightarrow ^3P_1$  ( $m_J=1$ )  $\rightarrow ^3S_1$  ( $m_J=1$ ) transition, and the magnetic trap is turned on around the optically prepared atoms. For a given  $^1S_0-^3P_1$  MOT population,  $N_T$ , the resulting magnetic trap population is  $f'N_T$  where here,  $f' \sim 0.3$ . Although the most technically challenging of all three transfer techniques, this approach has the benefit of producing ultracold ( $\sim 3 \mu\text{K}$  in the case of Sr [36]), large population ( $\sim 10^7$  atoms [10–12]) samples and is an attractive extension of the intercombination line laser cooling currently being pursued in Sr [10,11] and Yb [12]. Note, however, that type III transfer cannot be applied directly to Mg or Ca since in these cases,  $F_T \sim F_g/10$  where  $F_T$  ( $F_g$ ) is the  $^1S_0-^3P_1$  optical (gravitational) force and thus  $^1S_0-^3P_1$  MOTs cannot suspend Mg or Ca against gravity. For these two species, however, magnetic trapping of ultracold samples could be achieved by substituting the quenched narrow-line laser cooling technique recently developed by Curtis *et al.* [37] for the  $^1S_0-^3P_1$  MOT stage. Finally, we point out that due to the reduced sample temperatures achieved with type III transfer, Majorana flops will likely be a significant source of trap loss if the quadrupole magnetic field geometry assumed here is employed. This problem, however, can easily be overcome by switching in either rotating bias [38] or Ioffe [39] fields during the magnetic trapping stage.

For all three transfer schemes, zero-background detection of the magnetically trapped atoms can be realized via optical excitation of the  $^3P_2-^3S_1$  transition followed by selective observation of radiative decay from the  $^3S_1$  state to either the  $^3P_1$  state or the  $^3P_0$  state. Several factors, however, must be considered when performing these measurements. First, in contrast to traditional ground-state magnetically trapped alkali metal samples, the probability that a given atom will radiatively decay to untrapped states ( $^3P_1$  and  $^3P_0$ ) following excitation of the  $^3P_2-^3S_1$  transition is approximately 1 (see Fig. 3 and Ref. [32]). Consequently, detecting the magnetically trapped atoms requires efficiently collecting the  $^3S_1-^3P_{1,0}$  fluorescence. Additionally, although the  $^3S_1-^3P_2$  transition is spectrally separated from the  $^3S_1-^3P_1$  and  $^3S_1-^3P_0$  transitions by  $\Delta\lambda_d > 10$  nm in Yb and Sr, for Mg and Ca,  $\Delta\lambda_d \sim 1$  nm [24,25], requiring, for zero-background measurements, a spectrometer or an equivalent spectrally selective device. Note, however, that for sufficiently high spatial densities it may be possible to use the absorptive [7] or dispersive light scattering [40] techniques commonly employed to characterize magnetically trapped alkali metals.

Studies of laser cooled Yb and alkaline earth atoms have provided important insights into light-assisted collisions, radiation-pressure induced MOT density limits, and all-optical pathways to quantum degeneracy. We have presented and analyzed several novel strategies for efficiently loading-

these species into magnetic traps and demonstrated that significant trap populations can be obtained using  $^1S_0-^1P_1$  MOT magnetic fields and currently achieved  $^1S_0-^1P_1$  MOT populations. Our procedures may thus enable the uniquely simple yet versatile properties of Yb and the alkaline earths to be exploited in the ultracold, photon-free regime available in magnetic traps where evaporative cooling and ultimately-observations of quantum degeneracy in these species may be possible.

*Note added in proof.* Recently, refined values for the Mg, Ca, and Sr  $^3P_2$  state lifetimes have become available. See Ref. [41].

The authors wish to thank S. G. Porsev for calculating the Mg, Ca, and Sr  $^3P_2$  state radiative lifetimes and C. Greiner for helpful comments and suggestions. We gratefully acknowledge financial support from the National Science Foundation under Grant No. PHY-9870223.

- 
- [1] D. E. Pritchard, Phys. Rev. Lett. **51**, 1336 (1983); A. L. Migdall *et al.*, *ibid.* **54**, 2596 (1985).
- [2] E. Tiesinga, A. J. Moerdijk, B. J. Verhaar, and H. T. C. Stoof, Phys. Rev. A **46**, R1167 (1992); E. Tiesinga, B. J. Verhaar, and H. T. C. Stoof, *ibid.* **47**, 4114 (1993); S. Inouye *et al.*, Nature (London) **392**, 151 (1998); J. L. Roberts *et al.*, Phys. Rev. Lett. **81**, 5109 (1998).
- [3] C. R. Monroe *et al.*, Phys. Rev. Lett. **70**, 414 (1993); B. DeMarco *et al.*, *ibid.* **82**, 4208 (1999).
- [4] A. G. Martin *et al.*, Phys. Rev. Lett. **61**, 2431 (1988); K. Helmerson, A. Martin, and D. E. Pritchard, J. Opt. Soc. Am. B **9**, 483 (1992); **9**, 1988 (1992).
- [5] K. Helmerson, A. Martin, and D. E. Pritchard, J. Opt. Soc. Am. B **11**, 1988 (1992); N. R. Newbury, C. J. Myatt, E. A. Cornell, and C. E. Wieman, Phys. Rev. Lett. **74**, 2196 (1995).
- [6] H. F. Hess, Phys. Rev. B **34**, 3476 (1986); N. Masuhara *et al.*, Phys. Rev. Lett. **61**, 935 (1988); W. Ketterle and N. J. van Druten, in *Advances in Atomic, Molecular, and Optical Physics*, edited by B. Bederson and H. Walther (Academic, Boston, 1996), and references therein.
- [7] M. H. Anderson *et al.*, Science **269**, 198 (1995); C. C. Bradley, C. A. Sackett, J. J. Tollett, and R. G. Hulet, Phys. Rev. Lett. **75**, 1687 (1995); K. B. Davis *et al.*, *ibid.* **75**, 3969 (1995).
- [8] B. DeMarco and D. S. Jin, Science **285**, 1703 (1999).
- [9] N. Holden, in *Handbook of Chemistry and Physics*, 71st ed., edited by D. R. Lide (CRC, Boca Raton, FL, 1990).
- [10] K. Vogel, T. P. Dinneen, A. Gallagher, and J. L. Hall, in *International Quantum Electronics Conference*, Vol. 7, 1998 OSA Technical Digest Series (Optical Society of America, Washington, DC, 1998), pp. 223; K. R. Vogel, Ph.D thesis, University of Colorado, 1999 (unpublished).
- [11] H. Katori, T. Ido, Y. Isoya, and M. Kuwata-Gonokami, Phys. Rev. Lett. **82**, 1116 (1999); T. Ido, Y. Isoya, and H. Katori, Phys. Rev. A **61**, 061403(R) (2000).
- [12] T. Kuwamoto, K. Honda, Y. Takahashi, and T. Yabuzaki, Phys. Rev. A **60**, R745 (1999).
- [13] T. P. Dinneen *et al.*, Phys. Rev. A **59**, 1216 (1999); M. Machholm, P. S. Julienne, and K.-A. Suominen, *ibid.* **59**, R4113 (1999); G. Zinner, T. Binnewies, F. Riehle, and E. Tiemann, Phys. Rev. Lett. **85**, 2292 (2000).
- [14] T. Loftus, J. R. Bochinski, and T. W. Mossberg, Phys. Rev. A **63**, 053401 (2001).
- [15] For Yb, the  $^3P_2$  state radiative lifetime is  $\sim 15$  s. See Refs. [16] and [17]. For Mg, Ca, and Sr, the  $^3P_2$  radiative lifetimes are  $\sim 5000$ ,  $\sim 18\,000$ , and  $\sim 1200$  s, respectively. See Ref. [18].
- [16] S. G. Porsev, Yu. G. Rakhlina, and M. G. Kozlov, Phys. Rev. A **60**, 2781 (1999).
- [17] J. Migdalek and W. E. Baylis, J. Phys. B **24**, L99 (1991).
- [18] S. G. Porsev (private communication).
- [19] E. U. Condon and G. H. Shortley, *The Theory of Atomic Spectra* (The University Press, Cambridge, 1935), p. 76.
- [20] T. Bergman, G. Erez, and H. J. Metcalf, Phys. Rev. A **35**, 1535 (1987).
- [21]  $^1S_0-^1P_1$  Mg, Ca, and Sr MOTs use axial magnetic field gradients that range from 60 to 160 G/cm. See Refs. [11, 34] and T. Kurosu and F. Shimizu, Jpn. J. Appl. Phys., Part 1 **31**, 908 (1992). These larger gradients, however, simply increase the  $^3P_2$  ( $m_J=2$ ) magnetic trap depth beyond what is shown in Fig. 1.
- [22] In Sr, temperatures near the single-photon recoil temperature can be achieved. In this case, therefore, we use the 400 nK  $^1S_0-^3P_1$  MOT temperatures obtained in Ref. [11] for  $T_T$ .
- [23] T. Loftus, J. R. Bochinski, R. Shivitz, and T. W. Mossberg, Phys. Rev. A **61**, 051401(R) (2000).
- [24] W. C. Martin, R. Zalubas, and L. Hagan, in *Atomic Energy Levels-The Rare Earth Elements*, Natl. Bur. Stand. (U.S.) NSRDS-NBS 60 (U.S. GPO, Washington, DC, 1978); S. Bashkin and J. O. Stoner, *Atomic Energy Levels & Grotian Diagrams I* (American Elsevier, New York, 1976), p. 388; C. E. Moore, in *Atomic Energy Levels as Derived From the Analysis of Optical Spectra*, Natl. Bur. Stand. (U.S.) NSRDS-NBS 35 (U.S. GPO, Washington, DC, 1971).
- [25] NIST Atomic Spectra Databases, available in electronic form at <http://physics.nist.gov/PhysRef-Data/ASDA1/>.
- [26] J. E. Golub, Y. S. Bai, and T. W. Mossberg, Phys. Rev. A **37**, 119 (1988).
- [27] J. E. Hansen, J. Phys. B **11**, L579 (1978).
- [28] C. W. Bauschlicher, S. R. Langhoff, and H. Partridge, J. Phys. B **18**, 1523 (1985).
- [29] L. R. Hunter, W. A. Walker, and D. S. Weiss, Phys. Rev. Lett. **56**, 823 (1986).
- [30] R. Drozdowski, M. Ignaciuk, J. Kwela, and J. Heldt, Z. Phys. D: At., Mol. Clusters **41**, 125 (1997).
- [31] A. A. Radzig and B. M. Smirnov, *Reference Data on Atoms, Molecules, and Ions* (Springer-Verlag, Berlin, 1985), p. 222.
- [32] W. L. Wiese and G. A. Martin, in *Wavelengths and Transition Probabilities for Atoms and Atomic Ions*, Natl. Bur. Stand. (U.S.) NSRDS-NBS 68 (U.S. GPO, Washington, DC, 1980); L. Liljeby *et al.*, Phys. Scr. **21**, 805 (1980); A. Godone and C. Novero, Phys. Rev. A **45**, 1717 (1992); N. Beverini *et al.*, J. Opt. Soc. Am. B **11**, 2188 (1989).

- [33] A. Messiah, *Quantum Mechanics, Volume II* (Wiley, New York, 1962), p. 573.
- [34] K. Sengstock *et al.*, Opt. Commun. **103**, 73 (1993); K. Sengstock *et al.*, Appl. Phys. B: Lasers Opt. **59**, 99 (1994); F. Ruschewitz *et al.*, Phys. Rev. Lett. **80**, 3173 (1998).
- [35] T. Binnewies, U. Sterr, J. Helmcke, and F. Riehle, Phys. Rev. A **62**, 011601(R) (2000).
- [36] Using the 400 nK  $^1S_0 - ^3P_1$  MOT temperature reported in Ref. [11] and including loading induced photon recoil heating.
- [37] E. A. Curtis, C. W. Oates, and L. Hollberg, Phys. Rev. A **64**, 031403(R) (2001).
- [38] W. Petrich, M. H. Anderson, J. R. Ensher, and E. A. Cornell, Phys. Rev. Lett. **74**, 3352 (1995).
- [39] M.-O. Mewes *et al.*, Phys. Rev. Lett. **77**, 416 (1996).
- [40] M. R. Andrews *et al.*, Science **273**, 84 (1996).
- [41] A. Derevianko, Phys. Rev. Lett. **87**, 023002 (2001).